



Contents lists available at ScienceDirect

## Arabian Journal of Chemistry

journal homepage: [www.ksu.edu.sa](http://www.ksu.edu.sa)

# Synthesis of novel ursolic acid-gallate hybrids via 1,2,3-triazole linkage and its anti-oxidant and anti-inflammatory activity study

Zhiwen Qi<sup>a</sup>, Pujun Xie<sup>a</sup>, Zhihong Wang<sup>d</sup>, Hao Zhou<sup>a</sup>, Ran Tao<sup>a</sup>, Sergey A. Popov<sup>b,\*</sup>, Guliang Yang<sup>c,\*</sup>, Elvira E. Shults<sup>b</sup>, Chengzhang Wang<sup>a,\*</sup>

<sup>a</sup> Institute of Chemical Industry of Forest Products, Chinese Academy of Forest, Nanjing 210042, Jiangsu, China

<sup>b</sup> Novosibirsk Institute of Organic Chemistry, Acad. Lavrentyev Ave. 9, 630090 Novosibirsk, Russia

<sup>c</sup> National Engineering Laboratory for Rice and By-products Processing, Food Science and Engineering College, Central South University of Forestry and Technology, Changsha 410004, Hunan, China

<sup>d</sup> Guangdong Provincial Key Laboratory of Silviculture, Protection and Utilization, Guangdong Academy of Forestry, Guangzhou 510520, China

## ARTICLE INFO

## Keywords:

Ursolic acid

Gallic acid

Hybrids

Structure–activity relationships

Anti-inflammatory mechanism

## ABSTRACT

Excessive oxidation can lead to inflammation and affect health. Studies have shown that ursolic acid (UA) and gallic acid are widely employed in medicine and cosmetics owing to their obvious antioxidant and anti-inflammatory properties. In this study, a series of 16 novel UA hybrids tethered via 1,2,3-triazole to the modified gallate moieties were synthesized via CuAAC 1,3-cycloaddition reactions. *In vitro*, all derivatives were proved to be effective in antioxidation and anti-inflammation activities. Interestingly, compound **20** significantly inhibited the expression of pro-inflammatory cytokines including mRNA of inducible nitric oxide synthase (iNOS) ( $p < 0.05$ ) and cyclooxygenase-2 (COX-2) ( $p < 0.01$ ) in lipopolysaccharide (LPS)-induced RAW264.7 cells in a dose-dependent manner. The inhibitory effect of compound **20** on pro-inflammatory cytokines was closely associated with suppression of the LPS-activated PI<sub>3</sub>K/Akt signal pathway. Compound **20** significantly alleviated inflammation in the gastrointestinal tract of zebrafish *in vivo*. In addition, compound **20** showed good biosafety in cytotoxicity evaluation. This study provides a novel reference for the development of treatments for health problems related to anti-oxidation and anti-inflammation properties.

## 1. Introduction

Inflammation is a normal defensive response of the body to external stimuli. Once out of control, it can disrupt human function, referring to pathological conditions (Scotti et al., 2018). For example, lipopolysaccharide (LPS) is a polysaccharide component of the cell wall of Gram-negative bacteria. LPS-induced inflammatory response mainly induces macrophages and neutrophils to release inflammatory cytokines such as tumor necrosis factor, resulting in damage to the body. So far, abundant secondary metabolites from numerous herbal sources have attracted considerable attention to the design of anti-LPS-induced inflammatory drugs with low cytotoxicity and side effects (Lipeeva et al., 2020, Zhang et al., 2021).

In general, scavenging of excessive ROS and NO, and suppression of macrophage migration inhibitory factor (MIF) play a vital role in protecting cells and inhibition of lipid peroxidation (Sultana and Saeed Saify, 2012). The overproduction of NO and ROS is closely related to chronic inflammatory response, which can lead to serious diseases

(Sultana and Saeed Saify, 2012). The progression of these diseases can be effectively delayed or decreased by natural products through the PI<sub>3</sub>K/AKT signaling pathway (Quideau et al., 2011, Bilborrow et al., 2019).

To date, Ursolic acid (UA), as one of the most effective natural anti-inflammatory agents (Fig. 1), has attractive development and utilization potential (Al-kuraishy et al., 2022). The antioxidant and anti-inflammatory effect of UA are attributed to the inherent inhibition of enzymes involved in the generation of reactive oxygen species (ROS) and overexpression of nitric oxide (NO) (Checker et al., 2012, Habtemariam, 2019), increasing antioxidant enzyme activity, and reducing lipid peroxidation level. Moreover, UA exhibits a protective effect on lipopolysaccharide (LPS)-induced inflammation, resulting in suppression of proinflammatory cytokines and NO overproduction (Ryu et al., 2000, Wang et al., 2011, Chen et al., 2012) and the inhibition of LPS-induced nuclear factor kappa-B (NF-κB) activation and down-regulation of COX-2 (Shanmugam et al., 2012). However, the poor water solubility and low bioavailability of UA limit its clinical application.

\* Corresponding authors.

<https://doi.org/10.1016/j.arabjc.2024.105762>

Received 28 November 2023; Accepted 25 March 2024

Available online 26 March 2024

1878-5352/© 2024 The Authors. Published by Elsevier B.V. on behalf of King Saud University. This is an open access article under the CC BY-NC-ND license (<http://creativecommons.org/licenses/by-nc-nd/4.0/>).

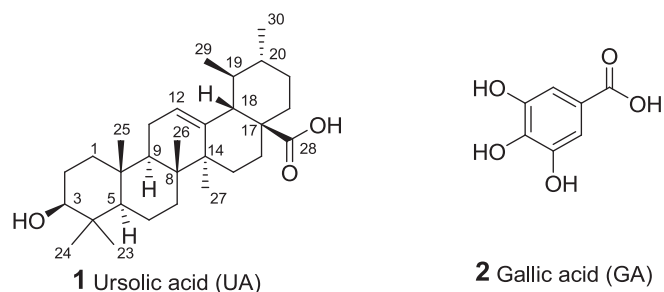


Fig. 1. The structures of ursolic acid and gallic acid.

Therefore, the development of new UA anti-inflammatory drugs with high efficiency has become an important issue to be solved.

Gallic acid (GA), which is widely available in nature (Fig. 1), has been shown to significantly attenuate the inflammatory response induced by LPS (Radtke et al., 2004). GA exhibits an obvious scavenging effect on 2,2-diphenyl-1-picrylhydrazyl (DPPH) free radicals, which is significantly higher than that of vitamin C (Vc) (Silva and Sirasa, 2018). GA inhibits lipid peroxidation in mice by anti-oxidation and has a therapeutic effect on cardiovascular disease. Furthermore, GA can reduce the expression levels of TNF- $\alpha$ , IL-1 $\beta$ , and IL-6 induced by LPS. LPS stimulation leads to increased expression of TLR4 mRNA and protein and activation of NF- $\kappa$ B (Zhu et al., 2019). GA can antagonize these effects and prevent NF- $\kappa$ B activation. In addition, GA alkyl esters have excellent oxidation resistance and are used as food antioxidants worldwide (Al Zahrani et al., 2020). The use of alkyl gallates often improves liposolubility and safety, thereby enhancing biological efficacy.

1,2,3-triazole has been proven to bind to many enzymes and receptors through noncovalent interactions, which may lead to enhanced anti-inflammatory activity (Gonzaga et al., 2017). The polar 1,2,3-triazole group can decrease the overall lipophilicity of triterpenoid hybrids (Csuk and Deigner, 2019; Lipeeva et al., 2020; Zhang et al., 2021). UA hybrids incorporating 1,2,3-triazoles were reported to exhibit noticeable anti-inflammatory activity (Csuk and Deigner, 2019; Lipeeva et al., 2020). Among various UA derivatives containing 1,2,3-triazole linker (Zhang et al., 2021), the UA hybrid with a polyphenol derivative with protected hydroxyl groups was a leader in anti-inflammation screening.

At present, synthetic conjugates are known in which the carboxamides of triterpene acid and polyphenolic acid are connected with polymethylene linkers, for which cytotoxic properties (Jiang et al., 2018) and antiviral activities (Li et al., 2019) have been revealed. There is only one known example of a hybrid of UA and a protected polyphenol tethered by 1,2,3-triazole (Zhang et al., 2021). For this reason, we attempted to synthesize new amphiphilic hybrids containing a lipophilic triterpene backbone, and a hydrophilic fragment including a polar gallate residue and 1,2,3-triazole linker. General, Cu-catalyzed 1,3-cycloaddition of substituted azides to terminal alkynes is a potent and versatile tool widely used in medicinal chemistry to develop novel bioactive products (Wang et al., 2014; Ke et al., 2018). Numerous variants of “click” method that use different Cu catalysts and solvents (Wang et al., 2014; Pucci et al., 2020) are known, including those that employ immobilized or supported catalysts (Wang et al., 2014; Liang et al., 2022). We assume that various binding modes of modified GA linked through 1,2,3-triazole to UA core will lead to novel hybrids with high antioxidant and anti-inflammatory activity.

In this paper, GA derivatives with alkyne and azide residues attached at the *meta*- and *para*- positions related to the carboxyl group of gallates, as well as at the carboxyl and propargyl group of GA, were used in the 1,3 cycloaddition reactions. UA esters and amides with terminal azides and propargyl groups were synthesized and used as intermediate compounds. Series of novel ester and amide hybrids substituted at C-28 of the UA core linked via 1,2,3-triazole with variously substituted modified

gallate moieties were prepared in CuAAC 1,3-cycloaddition reactions. Further, *in vitro* screening of hybrids in PI3K/AKT and MIF tautomerase assays, as well as cell safety, was explored. The anti-inflammatory effect of the best molecule was also evaluated in zebrafish. It is anticipated that drugs with enhanced activity and reduced toxicity in antioxidant and anti-inflammatory properties can be developed.

## 2. Materials and methods

### 2.1. Materials

All commercially available reagents were obtained from commercial sources and used without further purification. Reactions were monitored by thin-layer chromatography (TLC) in silica gel, and visualised by 254 nm ultraviolet light. Products were purified by flash column chromatography over silica gel (200–300 mesh). IR spectra were recorded on a Bruker Vector 22 FTIR spectrometer in KBr pellets. Mass spectra were recorded on a Thermo Fisher Scientific DFS high-resolution mass spectrometer (evaporator temperature 200–250 °C, electron ionization (EI) at 70 eV).  $^1\text{H}$  and  $^{13}\text{C}$  NMR spectra were registered on a Bruker AV-300 (300.13 MHz for  $^1\text{H}$ , 75.48 MHz for  $^{13}\text{C}$ ), Bruker AV-400 (400.13 MHz for  $^1\text{H}$ , 100.62 MHz for  $^{13}\text{C}$ ) and DRX-500 (operating frequencies 500.13 and 125.76 MHz, respectively) at room temperature. The chemical shifts are given in ppm relative to signals of the solvents used as internal standards: in  $^1\text{H}$  NMR spectra  $\delta\text{H}$  7.24 ( $\text{CHCl}_3$ ) and in  $^{13}\text{C}$  NMR spectra  $\delta\text{C}$  76.90 ( $\text{CDCl}_3$ ). Signals in the NMR  $^1\text{H}$  and  $^{13}\text{C}$  spectra of ursane series were assigned by correlation with those of ursolic acid (Sang et al., 2002) and ursolic acid acetate (Tkachev and Denisov, 1994). Signals in the NMR  $^1\text{H}$  and  $^{13}\text{C}$  spectra of lupane series were assigned by correlation with those of betulin and betulonic acid derivatives (Antimonova et al., 2013). *J* values are given in Hertz. The reaction progress was monitored by TLC on Sorbfil UV-254 plates using a methyl *tert*-butyl ether (MTBE)-hexane mixture as eluents, with visualization by a  $\text{FeCl}_3$  solution and under UV light. The reaction products were isolated by column chromatography using silica gel from Acros (35–70  $\mu\text{m}$ ). In the NMR  $^1\text{H}$  and  $^{13}\text{C}$  spectra, the assignments marked with the same symbols (§, #) are interchangeable.

The NO detection kit was purchased from Nanjing Jiancheng Bioengineering Institute. DPPH and vitamin C (Vc) were purchased from Aladdin Reagent Co., Ltd. (Shanghai, China). Vistusertib (AZD2014) was purchased from MedChemExpress Co., Ltd. (New Jersey, USA). Other reagents were of analytical pure and purchased from commercial reagent companies. RAW 264.7 and L929 cells were obtained from the China Center for Type Culture Collection (Wuhan, Hubei, China). Fetal bovine serum, DMEM high glucose medium, trypsin, and 100  $\times$  concentrated penicillin–streptomycin stock mixture was purchased from Gibco (Carlsbad, CA, USA). The primary antibodies of phospho-PI3 Kinase (#17366), PI3 Kinase p110  $\delta$  (#34050), Akt (#4691), phospho-Akt (#4060), COX-2 (#12282), iNOS (#13120), and  $\beta$ -Actin (#4970) were purchased from Cell Signaling Technology (Danvers, MA, USA). RIPA lysis (#sc-24948A) was purchased from Santa Cruz (Wuhan, Hubei, China). DNase I (#2270A), Advantage RT-for-PCR kit (#639505), and PrimeScript<sup>TM</sup> RT Master Mix kit (#RR036Q) were purchased from Takara (Dalian, Liaoning, China). Rosmanol (#HY-N5015) was purchased from MCE (Monmouth Junction, NJ, USA). Recombinant Human MIF Protein (hMIF, Shanghai Offshore Protein Technology Co., Ltd.).

### 2.2. Synthesis

#### Reaction of triterpenoid propargyl derivative with azides.

To a suspension of triterpenoid propargyl derivative **13** or **16** (0.5 mmol), in a mixture of *t*-BuOH (3 mL) and  $\text{H}_2\text{O}$  (1 mL) a solution of  $\text{CuSO}_4 \cdot 5\text{H}_2\text{O}$  (0.05 mmol) and sodium ascorbate (0.05 mmol) in  $\text{H}_2\text{O}$  (0.3 mL) was added and stirred for 0.5 h at ambient temperature followed by addition of azide **7a** or **7b** or 2-hydroxyethyl azide (0.5 mmol). The reaction mixture was stirred at ambient temperature for 10–24 h

(TLC control). The reaction mixture was poured into ice water, extracted with MTBE (3 × 30 mL). The organic phase was dried by anhydrous Na<sub>2</sub>SO<sub>4</sub> and concentrated in vacuum. The concentrate was chromatographed over silica gel column (SiO<sub>2</sub>, CH<sub>2</sub>Cl<sub>2</sub>-MTBE) to afford triterpenoid-gallic acid hybrids with triazole linkers.

**Methyl 3-(2-(4-((3β-hydroxyurs-12-en)-28-oyloxymethyl)-1H-1,2,3-triazol-1-yl)ethoxy)-4,5-((R,S)-methoxymethylenedioxy)-benzoate 19.**

Yield 69 % as off-white powder. IR (KBr)  $\nu$  max (cm<sup>-1</sup>): 661, 681, 731, 766, 785, 825, 868, 883, 914, 951, 995, 1032, 1107, 1142, 1182, 1194, 1228, 1246, 1302, 1319, 1344, 1365, 1383, 1439, 1510, 1608, 1635, 1674, 1720, 2872, 2928, 2949, 3151, 3433. NMR <sup>1</sup>H (400.13 MHz, CDCl<sub>3</sub>,  $\delta$ , ppm, J/Hz): 0.46–0.49 (3H, m, H-26<sup>β</sup>), 0.69 (3H, s, H-25<sup>β</sup>), 0.75 (3H, d, J = 6.5, H-30<sup>#</sup>), 0.79 (3H, s, H-24<sup>β</sup>), 0.85 (3H, m, H-29<sup>#</sup>), 0.90 (3H, s, H-23<sup>β</sup>), 0.97 (3H, s, H-27), 2.13 (1H, d, J<sub>18,19</sub> = 11.3, H-18), 3.12 (1H, t, J = 4.9, H-3), 3.37 (3H, m, CHOCH<sub>3</sub>), 3.80 (3H, m, COOCH<sub>3</sub>), 4.46 (2H, m, CH<sub>2</sub>CH<sub>2</sub>N), 4.70 (2H, m, CH<sub>2</sub>CH<sub>2</sub>N), 5.03–5.13 (2H, m, COOCH<sub>2</sub>), 5.13 (1H, m, H-12), 6.88 (1H, br.s, CH-OMe), 7.22 (2H, m, Ar-H), 7.76 (1H, d, J = 3.3, OCH<sub>2</sub>C = CH). NMR <sup>13</sup>C (125.76 MHz, CDCl<sub>3</sub>,  $\delta$ , ppm): 15.3 (C-25), 15.5 (C-24), 16.5 (C-26), 16.6 (C-26'), 16.8 (C-29), 18.1 (C-6), 21.0 (C-30), 23.0 (C-11), 23.3 (C-27), 24.0 (C-16), 27.0 (C-2), 27.7 (C-15), 28.0 (C-23), 30.4 (C-21), 32.8 (C-7), 36.4 (C-22), 36.7 (C-10), 38.4 (C-1), 38.6 (C-4), 38.6 (C-19), 38.9 (C-20), 39.3 (C-8), 39.3 (C-8'), 41.8 (C-14), 41.8 (C-14'), 47.3 (C-9), 47.9 (C-17), 49.5 (CH<sub>2</sub>CH<sub>2</sub>N), 50.3 (CHOCH<sub>3</sub>), 50.3 (CHOCH<sub>3</sub>'), 52.1 (COOCH<sub>3</sub>), 52.6 (C-18), 52.6 (C-18'), 55.0 (C-5), 57.1 (OCH<sub>2</sub>CH<sub>2</sub>), 68.0 (CH<sub>2</sub>OAr), 78.7 (C-3), 104.2 (Ar-6), 111.6 (Ar-2), 111.8 (Ar-2'), 120.3 (OCHO), 124.4 (Ar-1), 125 (N-CH), 125.1 (N-CH'), 125.5 (C-12), 137.7 (C-13), 137.8 (C-13'), 138.1 (Ar-4), 140.4 (CH<sub>2</sub>CN), 140.4 (CH<sub>2</sub>C'N), 143.2 (Ar-3), 147.3 (Ar-5), 147.3 (Ar-5'), 165.8 (ArCOOMe), 177.2 (C-28). Found, *m/z*: 789.4552 [M]<sup>+</sup>. C<sub>45</sub>H<sub>63</sub>O<sub>9</sub>N<sub>3</sub> Calculated, *m/z*: 789.4559.

**Methyl 3-(2-(4-((3β-acetoxurs-12-en)-28-oylaminomethyl)-1H-1,2,3-triazol-1-yl)ethoxy)-4,5-((R,S)-methoxymethylenedioxy)-benzoate 20.**

Yield 74 % as white powder. IR (KBr)  $\nu$  max (cm<sup>-1</sup>): 559, 609, 665, 733, 768, 808, 820, 868, 885, 916, 951, 972, 1005, 1036, 1107, 1146, 1192, 1248, 1300, 1319, 1342, 1369, 1439, 1510, 1610, 1637, 1722, 2874, 2949, 3149, 3417. NMR <sup>1</sup>H (400. MHz, CDCl<sub>3</sub>,  $\delta$ , ppm, J/Hz): 0.37–0.47 (3H, m, H-26<sup>β</sup>), 0.73–0.79 (9H, m, H-25<sup>β</sup>, H-30<sup>#</sup>, H-24<sup>β</sup>), 0.85–0.90 (6H, m, H-29<sup>#</sup>, H-23<sup>β</sup>), 0.95–1.05 (3H, m, H-27), 1.98 (3H, s, CH<sub>3</sub>CO), 3.39 (3H, m, CHOCH<sub>3</sub>), 3.82 (3H, m, COOCH<sub>3</sub>), 4.30–3.53 (5H, m, CONH-CH<sub>2</sub>, CH<sub>2</sub>CH<sub>2</sub>N, H-3), 4.68 (2H, m, OCH<sub>2</sub>CH<sub>2</sub>N), 5.22 (1H, m, H-12), 6.0 (1H, br.s, CON-H), 6.87 (1H, m, CH-OMe), 7.24 (1H, m, Ar-H), 7.42 (1H, m, Ar-H), 7.71 (1H, m, NHCH<sub>2</sub>C = CH). NMR <sup>1</sup>H (400.13 MHz, CDCl<sub>3</sub>,  $\delta$ , ppm, J/Hz): 15.3 (C-25), 16.1 (C-24), 16.2 (C-24'), 16.4 (C-26), 17.0 (C-29), 17.8 (C-6), 21.0 (C-30), 21.1 (C-CH<sub>3</sub>CO), 23.0 (C-27), 23 (C-27'), 23.0 (C-11), 23.3 (C-2), 24.7 (C-16), 27.5 (C-15), 27.5 (C-15'), 27.8 (C-23), 30.6 (C-21), 32.3 (C-7), 32.4 (C-7'), 34.6 (CONHCH<sub>2</sub>), 36.5 (C-10), 36.5 (C-10'), 36.8 (C-22), 36.8 (C-22'), 37.4 (C-4), 38 (C-1), 38.8 (C-19), 39.2 (C-8), 39.2 (C-8'), 39.5 (C-20), 42.1 (C-14), 47.2 (C-9), 47.2 (C-9'), 47.4 (C-17), 47.5 (C-17'), 49.4 (NCH<sub>2</sub>CH<sub>2</sub>O), 50.3 (CHOCH<sub>3</sub>), 50.4 (CHOCH<sub>3</sub>'), 52.1 (COOCH<sub>3</sub>), 53.4 (C-18), 54.9 (C-5), 67.9 (CH<sub>2</sub>OAr), 80.6 (C-3), 104.1 (Ar-6), 111.4 (Ar-2), 111.5 (Ar-2'), 120.3 (OCHO), 123.3 (NNCH), 123.4 (NNCH'), 124.4 (Ar-1), 125.9 (C-12), 138 (Ar-4), 138 (Ar-4'), 138.9 (C-13), 138.9 (C-13'), 140.4 (CH<sub>2</sub>C = CH), 140.5 (CH<sub>2</sub>C' = CH'), 144.6 (Ar-3), 147.2 (Ar-5), 147.2 (Ar-5'), 165.7 (Ar-COOMe), 170.8 (CH<sub>3</sub>CO), 178 (C-28). Found, *m/z*: 830.4818 [M]<sup>+</sup>. C<sub>47</sub>H<sub>66</sub>O<sub>9</sub>N<sub>4</sub>. Calculated, *m/z*: 830.4824.

**Methyl 3-(3-(4-((3β-hydroxyurs-12-en)-28-oyloxymethyl)-1H-1,2,3-triazol-1-yl)propoxy)-4,5-((R,S)-methoxymethylenedioxy)-benzoate 21.**

Yield 70 % as white powder. IR (KBr)  $\nu$  max (cm<sup>-1</sup>): 663, 679, 766, 822, 870, 883, 912, 951, 976, 997, 1034, 1105, 1142, 1182, 1194, 1227, 1246, 1302, 1319, 1344, 1365, 1439, 1510, 1608, 1635, 1720, 2098, 2872, 2928, 2947, 3145, 3431. NMR <sup>1</sup>H (400.13 MHz, CDCl<sub>3</sub>,  $\delta$ , ppm, J/Hz): 0.53 (3H, s, H-26<sup>β</sup>), 0.69 (3H, s, H-25<sup>β</sup>), 0.76 (3H, d, J = 6.5, H-

30<sup>#</sup>), 0.82 (3H, s, H-24<sup>β</sup>), 0.85 (3H, m, H-29<sup>#</sup>), 0.90 (3H, s, H-23<sup>β</sup>), 0.99 (3H, s, H-27), 2.12 (1H, d, J<sub>18,19</sub> = 10.7, H-18), 2.37 (2H, t, J = 5.4, NCH<sub>2</sub>CH<sub>2</sub>), 2.67 (1H, br.s., OH), 3.13 (1H, t, J = 5.3, H-3), 3.37 (3H, m, CHOCH<sub>3</sub>), 3.79 (3H, m, COOCH<sub>3</sub>), 4.05 (2H, m, NCH<sub>2</sub>CH<sub>2</sub>), 4.55 (2H, t, J = 5.4, CH<sub>2</sub>CH<sub>2</sub>CH<sub>2</sub>O), 5.05 (2H, m, ArOCH<sub>2</sub>), 5.13 (1H, m, H-12), 6.90 (1H, br.s, CH-OMe), 7.16 (1H, m, Ar-H), 7.23 (1H, m, Ar-H), 7.67 (1H, s, OCH<sub>2</sub>C = CH). NMR <sup>13</sup>C (100.62 MHz, CDCl<sub>3</sub>,  $\delta$ , ppm): 15.3 (C-25), 15.6 (C-24), 16.7 (C-26), 16.8 (C-29), 18.2 (C-6), 20.9 (C-30), 23.1 (C-11), 23.3 (C-27), 24 (C-6), 27.1 (C-2), 27.8 (C-15), 28 (C-23), 29.2 (NCH<sub>2</sub>CH<sub>2</sub>CH<sub>2</sub>), 30.4 (C-21), 32.9 (C-7), 36.4 (C-22), 36.8 (C-10), 38.6 (C-1), 38.6 (C-4), 38.7 (C-19), 38.9 (C-20), 39.4 (C-8), 41.9 (C-14), 46.7 (NCH<sub>2</sub>), 47.4 (C-9), 47.9 (C-17), 50.1 (CHOCH<sub>3</sub>), 51.9 (COOCH<sub>3</sub>), 52.7 (C-18), 55.1 (C-5), 57.2 (COOCH<sub>2</sub>-), 66.0 (ArOCH<sub>2</sub>), 78.3 (C-3), 103.5 (Ar-6), 111.5 (Ar-2), 120.5 (OCHO), 124.4 (Ar-1), 124.4 (N-CH = C), 125.6 (C-12), 137.9 (C-13), 138.2 (C-Ar-4), 141.3 (N-CH = C), 142.8 (C-Ar-3), 147.2 (C-Ar-5), 165.8 (C-Ar-COOMe), 177.0 (C-28). Found, *m/z*: 803.4701 [M]<sup>+</sup>. C<sub>46</sub>H<sub>65</sub>O<sub>9</sub>N<sub>3</sub> Calculated, *m/z*: 803.4715.

**Removal of dioxolane protective group at aromatic ring, deprotection of phenolic OH groups.**

To a stirred solution of 4,5-methoxymethylenedioxy derivative 19 or 21 or 23 (0.3 mmol) in *i*-PrOH (2.5 mL) concentrated AcOH (214 mg, 3.5 mmol) and water (0.2 mL) was added. The mixture was stirred under reflux for 1 h (TLC control). To the cooled mixture water (50 mL) and NaHCO<sub>3</sub> (0.29 g, 3.5 mmol) was added. The mixture was extracted with CHCl<sub>3</sub> (3 × 20 mL). The organic phase was dried (Na<sub>2</sub>SO<sub>4</sub>) and concentrated in vacuum. The concentrate was chromatographed over silica gel column (SiO<sub>2</sub>, CH<sub>2</sub>Cl<sub>2</sub>-MTBE) to afford corresponding 4,5-dihydroxy- derivatives.

**Methyl 3-(2-(4-((3-hydroxyurs-12-en)-28-oyloxymethyl)-1H-1,2,3-triazol-1-yl)ethoxy)-4,5-dihydroxybenzoate 19a.**

IR (KBr)  $\nu$  max (cm<sup>-1</sup>): 606, 623, 663, 756, 806, 829, 852, 916, 951, 997, 1011, 1030, 1043, 1076, 1107, 1142, 1227, 1269, 1342, 1439, 1516, 1606, 1718, 2872, 2928, 2949, 3149, 3398. NMR <sup>1</sup>H (300.13 MHz, CDCl<sub>3</sub>,  $\delta$ , ppm, J/Hz): 0.47 (3H, m, H-26<sup>β</sup>), 0.71 (3H, s, H-25<sup>β</sup>), 0.78–0.83 (6H, H-30<sup>#</sup>, H-24<sup>β</sup>), 0.90 (3H, m, H-29<sup>#</sup>), 0.94 (3H, s, H-23<sup>β</sup>), 1.01 (3H, s, H-27), 2.16 (1H, d, J<sub>18,19</sub> = 12.1, H-18), 3.16 (1H, t, J = 4.8, H-3), 3.85 (3H, s, COOCH<sub>3</sub>), 4.39 (2H, t, J = 4.3, CH<sub>2</sub>CH<sub>2</sub>N), 4.70 (2H, t, J = 4.3, CH<sub>2</sub>CH<sub>2</sub>OH), 5.14 (2H, m, ArOCH<sub>2</sub>), 5.17 (1H, t, J = 4.3, H-12), 5.74 (2H, br.s, OH), 7.36 (1H, d, J = 1.8, Ar-H), 7.71 (1H, s, Ar-H), 7.77 (1H, m, NC = CH). NMR <sup>13</sup>C (75.48 MHz, CDCl<sub>3</sub>,  $\delta$ , ppm): 15.2 (C-25), 15.5 (C-24), 16.5 (C-26), 16.8 (C-29), 18.0 (C-6), 20.9 (C-30), 23.0 (C-11), 23.2 (C-27), 23.9 (C-16), 26.8 (C-2), 27.7 (C-15), 27.9 (C-23), 30.4 (C-21), 32.7 (C-7), 36.4 (C-22), 36.6 (C-10), 38.4 (C-1), 38.5 (C-4), 38.6 (C-19), 38.8 (C-20), 39.2 (C-8), 41.8 (C-14), 47.2 (C-9), 48.0 (C-17), 49.5 (OCH<sub>2</sub>CH<sub>2</sub>N), 51.9 (COOCH<sub>3</sub>), 52.6 (C-18), 54.9 (C-5), 57.0 (OCH<sub>2</sub>CH<sub>2</sub>N), 68 (CH<sub>2</sub>OAr), 78.9 (C-3), 107.8 (Ar-6), 111.7 (Ar-2), 121.1 (Ar-1), 125.2 (N-C = H), 125.5 (C-12), 137.6 (C-13), 138.8 (C-Ar-4), 143.1 (CH<sub>2</sub>CN = ), 144.8 (Ar-3), 145.1 (Ar-5), 166.6 (ArCOOMe), 177.6 (C-28). Found, *m/z*: 747.4450 [M]<sup>+</sup>. C<sub>43</sub>H<sub>61</sub>O<sub>8</sub>N<sub>3</sub> Calculated, *m/z*: 747.4453.

**Methyl 3-(3-(4-((3β-hydroxyurs-12-en)-28-oyloxymethyl)-1H-1,2,3-triazol-1-yl)propoxy)-4,5-dihydroxybenzoate 21a.**

Yield 92 % as off-white powder. IR (KBr)  $\nu$  max (cm<sup>-1</sup>): 661, 764, 787, 827, 874, 912, 951, 974, 997, 1009, 1030, 1090, 1101, 1140, 1200, 1225, 1267, 1340, 1439, 1516, 1606, 1716, 2098, 2874, 2929, 2949, 3147, 3398. NMR <sup>1</sup>H (300.13 MHz, CDCl<sub>3</sub>,  $\delta$ , ppm, J/Hz): 0.51 (3H, s, H-26<sup>β</sup>), 0.71 (3H, s, H-25<sup>β</sup>), 0.78 (3H, d, J = 6.3, H-30<sup>#</sup>), 0.81 (3H, s, H-24<sup>β</sup>), 0.88 (3H, m, H-29<sup>#</sup>), 0.93 (3H, s, H-23<sup>β</sup>), 1.00 (3H, s, H-27), 2.14 (1H, d, J<sub>18,19</sub> = 11.2, H-18), 2.33 (2H, m, J = 5.4, NCH<sub>2</sub>CH<sub>2</sub>), 2.67 (1H, br.s., OH), 3.18 (1H, m, H-3), 3.81 (3H, m, COOCH<sub>3</sub>), 4.05 (2H, m, NCH<sub>2</sub>CH<sub>2</sub>), 4.59 (2H, t, J = 5.4, CH<sub>2</sub>CH<sub>2</sub>CH<sub>2</sub>O), 5.11 (2H, m, ArOCH<sub>2</sub>), 5.16 (1H, m, H-12), 6.51 (1H, br.s, OH), 7.15 (1H, s, Ar-H), 7.31 (1H, m, Ar-H), 7.63 (1H, s, OCH<sub>2</sub>C = CH), 7.31 (1H, m, Ar-H), 7.97 (1H, br.s, OH). 15.3 (C-25), 15.5 (C-24), 16.7 (C-26), 16.8 (C-29), 18.1 (C-6), 21 (C-30), 23.1 (C-11), 23.3 (C-27), 24 (C-16), 26.9 (C-2), 27.8 (C-15), 27.9 (C-23), 29.6 (C-NCH<sub>2</sub>CH<sub>2</sub>-), 30.4 (C-21), 32.8 (C-7), 36.4 (C-22), 36.7

(C-10), 38.4 (C-1), 38.5 (C-4), 38.6 (C-19), 38.8 (C-20), 39.3 (C-8), 41.8 (C-14), 47.0 (NCH<sub>2</sub>CH<sub>2</sub>-), 47.3 (C-9), 48 (C-17), 51.9 (COOCH<sub>3</sub>), 52.6 (C-18), 55 (C-5), 57 (COOCH<sub>2</sub>-), 66.2 (CH<sub>2</sub>OAr), 78.9 (C-3), 107.8 (Ar-6), 111.3 (Ar-2), 121.1 (Ar-1), 124.6 (N-HC = C), 125.5 (C-12), 137.8 (C-13), 138.6 (Ar-4), 143.3 (N-HC = C), 144.6 (Ar-3), 145.4 (Ar-5), 166.7 (ArCOOMe), 177.5 (C-28). Found, *m/z*: 761.4608 [M]<sup>+</sup>. C<sub>44</sub>H<sub>63</sub>O<sub>8</sub>N<sub>3</sub> Calculated, *m/z*: 761.4610.

### 2.3. Biological activities assay

#### 2.3.1. Cell culture

Mouse RAW264.7 cells were cultured in Dulbecco's Modified Eagle Medium (Hyclone, USA) with 10 % fetal bovine serum, 100 U/mL penicillin and 100 µg/mL streptomycin (Beyotime, China) at 37°C in a humid environment containing 5 % CO<sub>2</sub>. All the cells used in the experiment are in the logarithmic growth stage with a 70–80 % confluency.

#### 2.3.2. In vitro DPPH free radical scavenging experiment

A certain concentration of hybrids was added to the mixture: 0.4 mmol/L DPPH in ethanol solution-20 mM Tris-HCl buffer (pH 7.4) (volume ratio 2:1). The free DPPH radical changes were determined by spectrophotometry after the dark reaction at room temperature of hybrids (5–50 µM) for 30 min. The final concentration of hybrids and the positive control Vc were 5, 10, 30, 50 µM respectively. The absorbance value was detected at 517 nm, including blank control A<sub>b</sub> and samples A<sub>s</sub>. The DPPH free radical scavenging rate was calculated according to the following formula. DPPH Free radical scavenging rate (%) = (A<sub>b</sub>-A<sub>s</sub>)/A<sub>b</sub> × 100 %.

#### 2.3.3. Inhibition of NO production

RAW264.7 cells were seeded in 96-well plates, and treated following grouped after reaching about 80 % confluence. The cells in the blank group were cultured in the medium containing 0.1 % DMSO, and the LPS stimulation group was added more LPS 500 ng/mL than the blank group. The concentration of the drug group was adjusted according to the results of the MTT experiment. After 24 h of intervention, 70 µL culture medium supernatant was extracted, and the NO scavenging efficiency of each treatment was carried out in strict accordance with the instructions of the NO assay kit (Cat#: A013-2-1, Nanjing Jiancheng Bioengineering Institute, Nanjing, Jiangsu, China). The absorbance value was measured by an MK3-Microplate Reader (LabSystems, Helsinki, Finland). The inhibition rates of NO production by different concentrations of each compound were calculated. NO production inhibition rate (%) = (LPS stimulation group-compound intervention group)/(LPS stimulation group- blank group) × 100 %.

#### 2.3.4. Cytotoxicity

Cell viability studies induced by compounds were evaluated by MTT assay. 100 µL/well RAW264.7 were seeded in 96-well plates at a density of 1 × 10<sup>4</sup> cells/mL in complete medium and incubated for 24 h. Then the cells were treated with compounds (25 µM) for 24 h. MTT (5 mg/mL in PBS, 10 % total volume) was added to each well and the cells were further incubated for 4 h. The supernatant was removed and 150 µL/well DMSO was added. The optical density was measured at 570 (Measurement wavelength) and 630 (reference wavelength) nm on a microplate reader (Thermo Scientific, Waltham, MA, USA).

#### 2.3.5. In vitro experimental grouping

When RAW264.7 cells grew to about 80 % confluence, five cell treatment groups were set up as follows: control group (CON), LPS + UA group (LPS + UA, 500 ng/mL LPS + 12 µg/mL UA), LPS group (LPS, 500 ng/mL LPS), LPS + Cpd 20 group (LPS + Cpd 20, 500 ng/mL LPS + 13.57 µg/mL Cpd 20), and LPS + rosmanol group (LPS + Rosm, 500 ng/mL LPS + 14.5 µg/mL rosmanol).

**Table 1**

Primers used in this study.

	Forward (5'- 3')	Reverse (5'- 3')
TNF-α	GGTGCCATATGTCTCAGCCTC	GCCATAGAAGCTGATGAGAGG
IL-6	TACCACTTCACAAGTCGGAG	TGCCAGTGAGCTTCCCCTTC
iNOS	CAGCTGGGCTGTACAAACCTT	CATTGGAAGTGAAGCGTTTCG
GAPDH	ATCACTGCCACCCAGAAGAC	TGCCAGTGAGCTTCCCCTTC

#### 2.3.6. Reverse transcription-polymerase chain reaction

After being treated with the corresponding compounds according to the experimental design for 24 h, the cells were collected and the total RNA was extracted. DNase I without RNase was used to eliminate the remaining genomic DNA, and then mRNA was reversely transcribed into cDNA. The transcription levels of TNF-α, IL-6 and iNOS were detected with a real-time PCR detection reagent. The relative expression levels were calculated via the 2<sup>-ΔΔCt</sup> method. The primer sequence was shown in Table 1.

#### 2.3.7. Protein collection and Western blotting assay

After being cultured respectively for 24 h, the total proteins of each group were extracted by RIPA lysis, and then denatured after quantitative analysis. After separation with sodium dodecyl sulfate-polyacrylamide gel electrophoresis (SDS-PAGE), the target bands were transferred onto polyvinylidene difluoride membranes. The combination of the associated primary and secondary antibodies was performed using conventional methods. The luminous reaction was performed with the enhanced chemiluminescence Western blotting substrate. Both image collection and quantitative gray value of target bands were carried out by the BIO-RAD ChemiDoc XRS imaging system (Hercules, CA, USA).

#### 2.3.8. Detection of reactive oxygen species levels

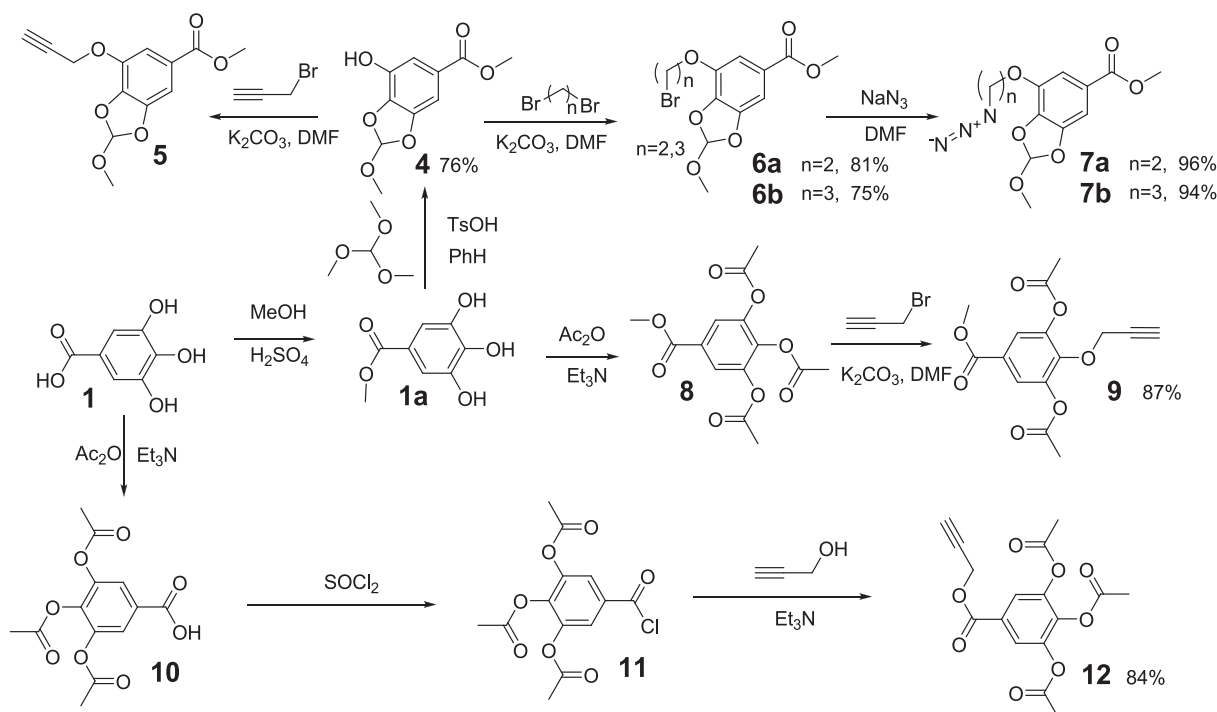
After being cultured for 24 h, the cell culture medium was replaced by serum-free culture medium supplemented with a ratio of 1/1000 2',7'-dichlorodihydrofluorescein diacetate (H2DCFHDA), and then incubated continuously at 37 °C for another 20 min. In the meantime, ROS levels were also detected by a flow cytometry (Beckman Coulter CytoFLEX, Brea, CA, USA).

#### 2.3.9. Detection of hydroxyl radical in LPS-stimulated zebrafish

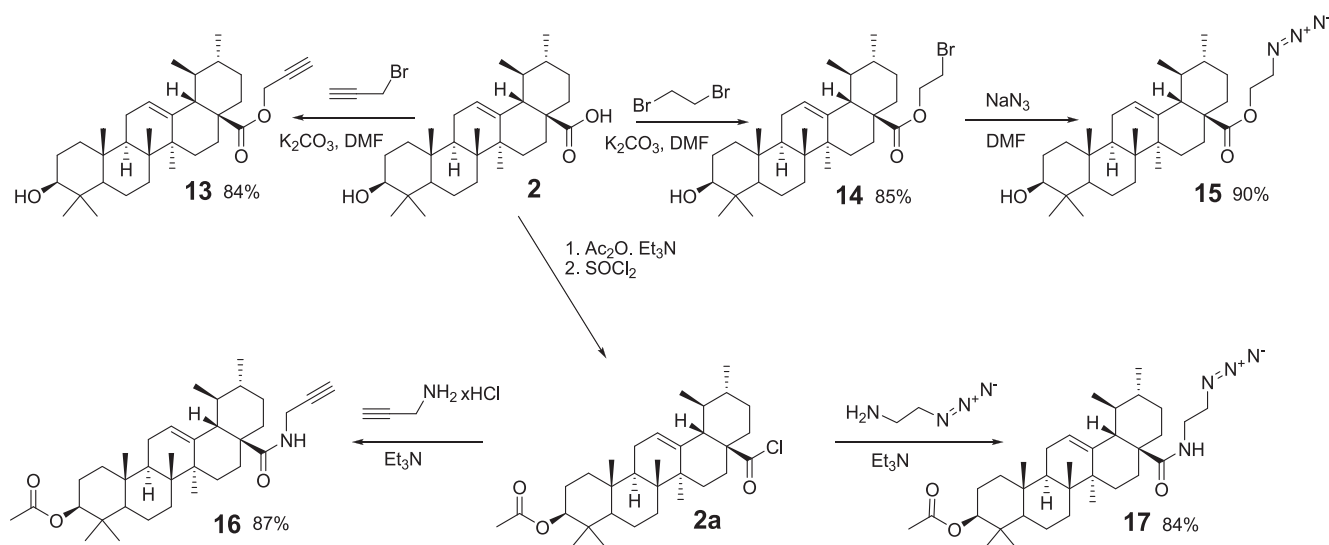
Zebrafish fertilized eggs were first incubated in embryonic medium (13.7 mM NaCl, 540 µM KCl, 25 µM Na<sub>2</sub>HPO<sub>4</sub>, 44 µM KH<sub>2</sub>PO<sub>4</sub>, 300 µM CaCl<sub>2</sub>, 100 µM MgSO<sub>4</sub>, 420 µM NaHCO<sub>3</sub>, pH 7.4) at 28.0°C. Six-day old zebrafish were used for inflammation induction experiments. 10 µg/mL LPS was added to the culture medium to induce gastrointestinal inflammation in zebrafish for 24 h. Then, in the screening of anti-inflammatory effects of drugs, the tested drug was co-cultured with zebrafish induced by inflammation for 24 h, and then DCFH (10 µM) was added for incubation for 4 h for imaging. The control group did not need drug pre-treatment. The co-culture method and probe processing time will be adjusted according to the experimental results, and then fluorescence imaging of zebrafish *in vivo*. Before zebrafish imaging, 10 % glycerol aqueous solution containing ethyl *m*-aminobenzoate (Tricaine, 150 µg/mL) was used for progressive anaesthesia and fixation. Fluorescence photos were quantitatively analysed by Image J software.

### 2.4. Statistical analysis

The octanol-water partition coefficient (AlogP) was calculated by Gaussian16 & Gaussian View6 (Gaussian, Inc., USA). The data are the mean ± SEM of 3 independent experiments. Data were analyzed using one-way ANOVA and Dunnett's test. SPSS Statistics 17.0 (SPSS Inc., Chicago, IL, USA) was used. All results were presented as mean ± SEM (n = 3). \**p* < 0.05, \*\*\**p* < 0.001, and \*\*\*\**p* < 0.0001 respectively indicate significant difference and statistically significant difference.



Scheme 1. Synthesis of propargyl- and azide- substituted derivatives of gallic acid.



Scheme 2. Synthesis of propargyl and azide derivatives of ursolic acid.

### 3. Results and discussion

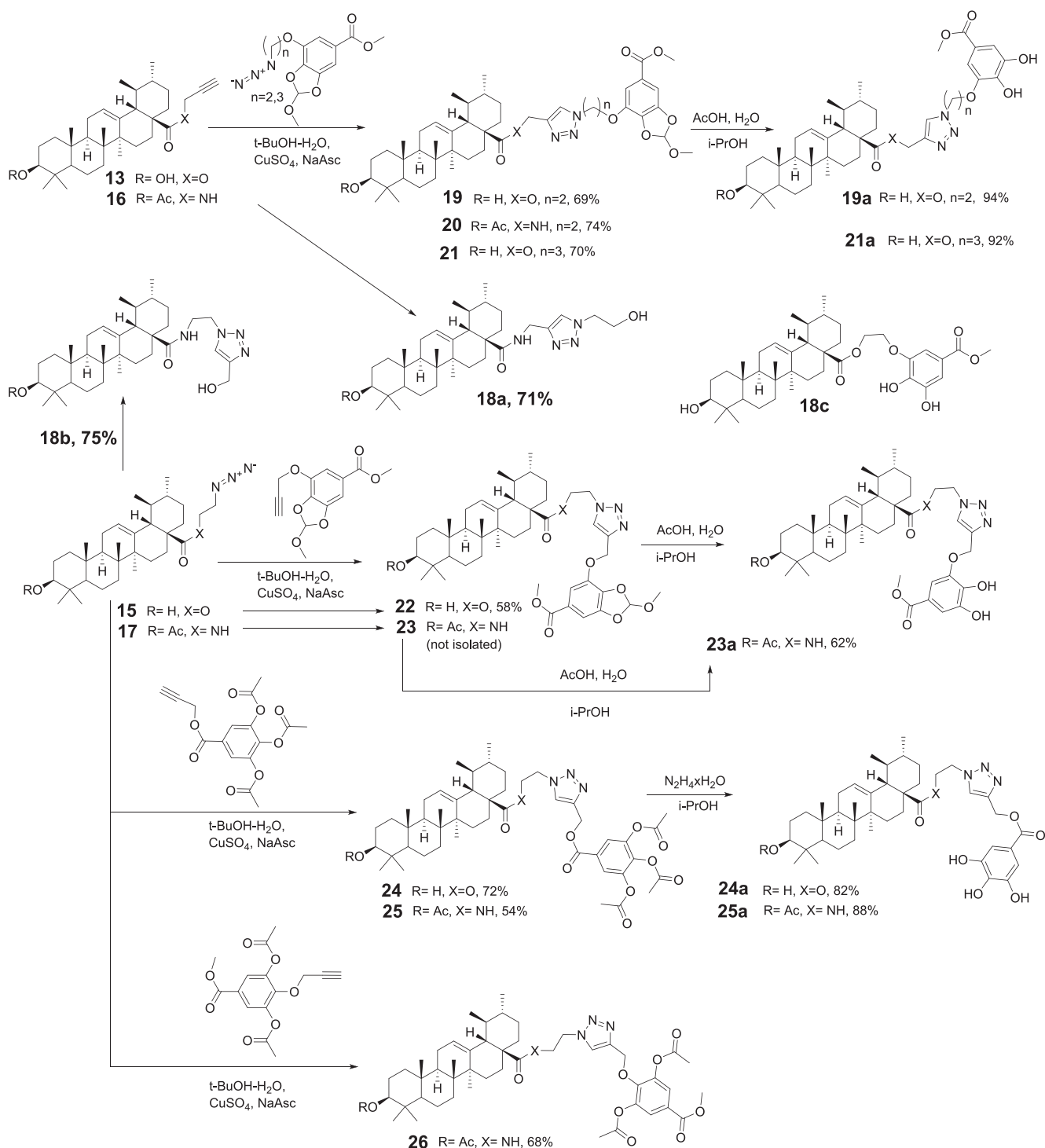
#### 3.1. Chemistry

The synthetic pathways employed for the synthesis of the intermediate and final compounds are depicted on the Schemes 1-3. Alkylation of methyl 3-hydroxy-4,5- ((R,S)-methoxymethylenedioxy) benzoate **4** and methyl 3,4,5-triacetoxybenzoate **8** with propargyl bromide in DMF in the presence of  $K_2CO_3$  afforded propargyl ethers **5** and **9** (yields 84 % and 87 %, respectively) with substituents at various positions of the protected gallate moieties (Scheme 1).

Propargyl ester **12** (91 %) was synthesized by the acylation of propargyl alcohol with 3,4,5-triacetoxybenzoyl chloride **11** (Scheme 1). In the reactions of bromides **6a**, **6b** with sodium azide in DMF, azides **7a**,

**7b** derived from OH-protected derivatives of gallic acid were obtained (96 % and 94 %). In a similar manner, 2-azidoethylursolate **15** (90 %) was synthesized from 2-bromoethylursolate in the reaction with  $NaN_3$  (Scheme 2). Derivatives of ursane C-28 amides with a propargyl substituent **16** and a 2-azidoethyl substituent **17** were obtained by reacting propargylamine and 2-aminoethyl azide with ursoloyl chloride acetate **2a** (87 % and 84 %).

1,3-cycloaddition reactions of ursane-type derivatives containing terminal acetylenic (**13**, **16**) or azide- substituents (**15**, **17**) at C-28 and the corresponding azides **7a**, **7b** or propargyl derivatives of polyphenols **5**, **9**, **12** were carried out at ambient temperature in the *t*-BuOH- $H_2O$  system in the presence of  $CuSO_4$ -sodium ascorbate. As a result, hybrids **19-26** were synthesized (54-74 %), which included an ester or amide group at C-28 of the triterpenoid linked through a 1,2,3-triazole-



**Scheme 3.** Scheme for the synthesis of UA-GA conjugates tethered by 1,2,3-triazole linkers. \* Synthetic details are given in supplementary information (S.I).

containing linker attached at different positions of the OH-protected polyphenol substituent (Scheme 3). The structures of the all compounds were confirmed by  $^1\text{H}$  NMR/ $^{13}\text{C}$  NMR and HRMS (see supplementary information).

The methoxymethylene protecting group in compounds **19**, **21**, **23** was removed by hydrolysis in the AcOH-H<sub>2</sub>O-*i*-PrOH system to achieve dihydroxy derivatives **19a**, **21a**, **23a** in excellent yields (92–94 %). Derivatives with free phenolic hydroxyls **24a**, **25a** (82 %, 88 %) were obtained by selective hydrazinolysis of acetyl groups at polyphenol, while the ester groups at triterpenoid remained intact.

### 3.2. *In vitro* DPPH radical and NO scavenging, MIF inhibition activity

In order to eliminate interference factors, all hybrid solutions were first scanned in the full wavelength range (200–800 nm). The maximum absorption for all tested compounds was found to range 235 to 245 nm, which would not interfere with the determination results. Therefore, it was feasible to assess the radicals of DPPH and NO scavenging capacity of all hybrids by colorimetry. As shown in Table 2, hybrids demonstrated different levels of DPPH and NO scavenging within the tested concentration range ( $p < 0.05$ ). The DPPH radical (half maximal inhibitory

**Table 2**

*Ex vivo* DPPH scavenging, *in vitro* IC<sub>50</sub>, NO removal and MIF suppression values of triterpenoid-gallic hybrids (unit:  $\mu\text{M}$ , Mean  $\pm$  SD, n = 3).

Entry	AlogP	DPPH	NO	MIF	IC <sub>50</sub>
17	–	24.56 $\pm$ 0.37	NA <sup>100</sup>	NA <sup>100</sup>	NA <sup>100</sup>
18a	–	18.72 $\pm$ 1.09	NA <sup>100</sup>	76.90 $\pm$ 4.68	NA <sup>100</sup>
18b	–	24.16 $\pm$ 0.26	NA <sup>100</sup>	NA <sup>100</sup>	NA <sup>100</sup>
18c	–	3.57 $\pm$ 0.52	45.09 $\pm$ 3.96	35.61 $\pm$ 2.69	30.99 $\pm$ 3.65
19	–	15.54 $\pm$ 0.22	NA <sup>100</sup>	84.30 $\pm$ 4.73	NA <sup>100</sup>
19a	–	3.45 $\pm$ 0.16	41.75 $\pm$ 1.76	53.62 $\pm$ 4.26	34.88 $\pm$ 2.98
20	8.348	1.61 $\pm$ 0.08	26.10 $\pm$ 2.38	21.40 $\pm$ 1.49	22.62 $\pm$ 3.65
21	8.678	2.19 $\pm$ 0.11	16.18 $\pm$ 1.13	35.26 $\pm$ 3.78	20.06 $\pm$ 1.74
21a	–	3.86 $\pm$ 0.10	44.48 $\pm$ 3.91	42.10 $\pm$ 3.38	34.54 $\pm$ 3.84
22	–	5.04 $\pm$ 0.44	50.35 $\pm$ 2.40	68.98 $\pm$ 5.98	49.82 $\pm$ 3.54
23a	–	2.31 $\pm$ 0.27	31.84 $\pm$ 1.72	46.32 $\pm$ 3.74	25.51 $\pm$ 1.23
24	–	6.96 $\pm$ 0.23	92.33 $\pm$ 4.72	NA <sup>100</sup>	92.68 $\pm$ 4.32
24a	7.477	2.07 $\pm$ 0.14	26.64 $\pm$ 1.70	29.26 $\pm$ 1.97	21.64 $\pm$ 2.01
25	–	7.37 $\pm$ 0.27	93.71 $\pm$ 6.23	98.60 $\pm$ 5.56	94.94 $\pm$ 5.28
25a	–	3.05 $\pm$ 0.18	35.28 $\pm$ 2.59	36.10 $\pm$ 2.84	30.14 $\pm$ 2.31
26	–	17.02 $\pm$ 0.15	NA <sup>100</sup>	NA <sup>100</sup>	NA <sup>100</sup>
UA	–	NA <sup>100</sup>	NA <sup>100</sup>	NT	29.95 $\pm$ 3.04
GA	–	9.30 $\pm$ 0.82	NA <sup>100</sup>	NT	NT
Vc	–	21.92 $\pm$ 0.34	NA <sup>100</sup>	NT	NT
Perifosine <sup>[b]</sup>	–	NT	23.18 $\pm$ 2.25	NT	NT
ISO-1 <sup>[c]</sup>	–	NT	NT	16.70 $\pm$ 1.35	NT

\*a. “NT”: non tested. “NA<sup>100</sup>”: the bio-viability was more than 70 % up to the highest tested concentration of 100  $\mu\text{g}/\text{mL}$  or  $\mu\text{M}$  (in superscript). b. Perifosine is a novel Akt inhibitor with an IC<sub>50</sub> of 4.7  $\mu\text{M}$  in MM.1S cells (Liu et al., 2021). c. ISO-1 is MIF antagonist as positive control.

concentration (IC<sub>50</sub>) clearance rate ranged from 1.61  $\pm$  0.08 to 24.56  $\pm$  0.37  $\mu\text{M}$ , compared to the blank control. The DPPH scavenging ability for certain compounds indicated a concentration-dependent manner ( $p < 0.05$ ) especially, and the IC<sub>50</sub> of compounds **20** was 1.61  $\pm$  0.08  $\mu\text{M}$ , significantly higher than that of positive control antioxidant Vc (21.92  $\pm$  0.34  $\mu\text{M}$ ). *In vitro*, the NO clearance IC<sub>50</sub> rate of all the hybrids was almost ranged from 16.18  $\pm$  1.13 to 93.71  $\pm$  6.23  $\mu\text{M}$ , implying a concentration-dependent manner ( $p < 0.05$ ). The clearance rates of several hybrids reached the level of the positive control perifosine (IC<sub>50</sub>: 23.18  $\pm$  2.25  $\mu\text{M}$ ). The release of NO in LPS-stimulated RAW264.7 cells was significantly inhibited after the intervention of compound **20** (26.10  $\pm$  2.38  $\mu\text{M}$ ) for 24 h, which was comparable with the results for perifosine.

In addition, macrophage MIF was assessed. MIF is regarded as an attractive anti-inflammatory target involved in the regulation of both the innate and the adaptive immune responses (Trivedi-Parmar and Jorgensen, 2018). The *in vitro* enzyme-based assay identified that some hybrids exhibited proximal potent inhibitory activity against MIF, compared with the positive control ISO-1 (IC<sub>50</sub>: 16.70  $\pm$  1.35  $\mu\text{M}$ ). For instance, compound **20** possessed the strongest inhibitory activity, and its MIF IC<sub>50</sub> value was estimated (21.40  $\pm$  1.49  $\mu\text{M}$ ) in a concentration-

dependent manner ( $p < 0.05$ ). It should be noted that both UA showed extremely poor DPPH inhibition and NO suppression, while GA did not suppress NO release. UA may even exhibit NO stimulating effect in RAW264.7 cells (Zhang et al., 2017). *In vitro* cytotoxicity test results for these compounds with the RAW264.7 cell line revealed that the semi-inhibitory concentrations of all hybrids on cell proliferation were significantly superior to those for DPPH inhibition and were close to those for NO and MIF inhibition.

In addition, to ensure bio-safety and avoid false positive results of these compounds, the MTT assay was carried out to screen the cytotoxicity against RAW264.7 cells for 24 h below the concentration of 100  $\mu\text{M}$ . In accordance with the MTT assay, hybrids were confirmed to have more potent inhibitory activity to RAW264.7 cells. As mentioned above, anti-inflammatory hybrids, including lead compounds **20**, **24a**, showed a stronger inhibitory effect on RAW264.7, in contrast to the parent compound.

### 3.3. Structure-Activity relationships (SAR)

As shown in Scheme 3, among C-28 substituted esters and amides of the UA core, hybrids **20** (amide), **21** (ester), and **24a** (ester) showed the highest inhibition in terms of DPPH, NO and MIF. UA do not contain a modified gallic acid moiety and exhibit weak antioxidant activity and poorly inhibited NO and MIF. Hybrid UA and GA, connected through an ethylene bridge (Popov et al., 2021a; Popov et al., 2021b) but not containing triazole, showed high antioxidant and moderate anti-inflammatory (NO, MIF) activity. At the same time, the results obtained for **18c** were significantly inferior to the data for the most active triterpenoid and GA hybrids tethered with a triazole linker (compounds **20**, **24**). Thus, the presence of both modified polyphenol fragments and 1,2,3-triazole in a hybrid triterpenoid molecule are important factors for antioxidant and anti-inflammatory activity.

Additionally, when triazole was combined with 3-hydroxy-4,5-((R, S)-methoxymethylenedioxy) benzoate moiety, two or three methylene linkages were essential for enhancing activity. When triazole is combined with gallic acid, biological activity can be increased by methylene connection (Popov et al., 2021a; Popov et al., 2021b, Qi et al., 2021). Especially, amide **20** (derived from propargyl amide **16**) was significantly superior to amides **23**, **25**, **26** (obtained from amide **17** with terminal azide) in these activities, and was also significantly better than esters **19**, **19a** and **21a** (derived from propargyl ester **13**).

In addition, the elongation of the aliphatic linker between 1,2,3-triazole and the aromatic substituent led to an improvement in antioxidant and anti-inflammatory activity (compound **21** (n = 3) vs compound **19** (n = 2)). However, among the studied UA-GA hybrids with a triazole linker, ester **22** (obtained from precursor azide **15**) and *para*-attached 3, 5-diacetate **26** (obtained from precursor azide **17**) were the least active. Increasing the length of the alkane chain between triazole and gallic acid (n = 2, 3) appropriately can maintain the normal conformation of the building block molecule and significantly improve biological activity (Popov et al., 2021a; Popov et al., 2021b), which is consistent with the activity of the UA biotin molecule (Qi et al., 2021).

Factors contributing to high anti-inflammatory activity of novel compounds may include the following: 1. A combination of triazole and gallate moieties as polar groups and a nonpolar triterpene backbone can lead to conjugates with amphiphilic properties. This can improve the solubility and bioavailability of hybrid derivatives. 2. The presence of two adjacent polar substituents in the aromatic fragment (compounds **20**, **24a**) is a factor accompanying the high anti-inflammatory action of hybrid triterpene derivatives with a triazole linker, which is consistent with literature data (Zhang et al., 2021). 3. The introduction of gallate moiety into the hybrid molecule provided excellent antioxidant properties, which may be responsible for the suppression of ROS. 4. The introduction of protected gallates with methoxymethylenedioxy moiety contributed to an increase in both anti-oxidant and anti-inflammatory activity. Compound containing the methoxymethylenedioxy moiety

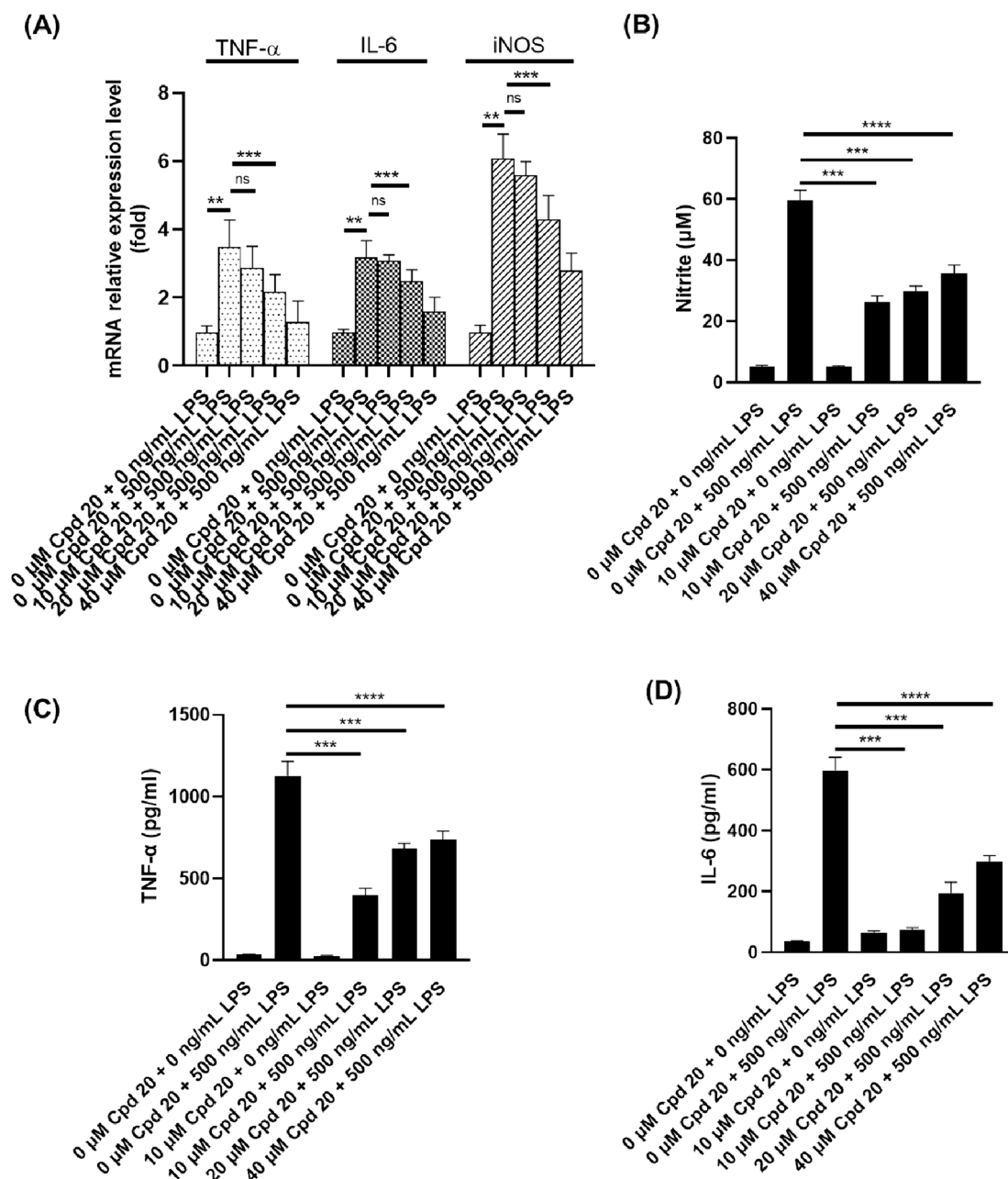


**Fig. 2.** Cpd20 downregulated the LPS-induced nitric oxide level and inflammatory factors level *in vitro*. (A) Transcriptional levels of TNF- $\alpha$ , IL-6 and iNOS; (B) Production of nitric oxide (NO); Levels of TNF- $\alpha$  (C) and IL-6 (D). Values are expressed as mean  $\pm$  SEM,  $n \geq 3$ . ns represents non-significant difference. \* Represents significant differences, \*\* $p < 0.01$ , \*\*\* $p < 0.001$ , \*\*\*\* $p < 0.0001$ .

may be regarded as a latent form of both a polyphenol and an aldehyde. According to literature data, introduction of 1,3-benzodioxole moieties can provide compounds with enhanced anti-oxidant, anti-inflammatory (COX-2 inhibitors) and hypolipidemic effects (Hawash et al., 2020, Xie et al., 2021). Thus, the antioxidant activity of hybrids with 1,3-dioxolane protection, may exceed the corresponding results for derivatives with free phenolic OH groups. 5. The ester or amide bond between the C-28 of the UA and the linker, as well as the ether bond between the linker and the gallate moiety, are resistant to hydrolysis, which ensures the stability of hybrid derivatives.

#### 3.4. Downregulation of RAW264.7 cell oxidation level through the PI3K/AKT pathway

Compound-leader **20**, which exhibited the most potent MIF

inhibition was selected to further investigate the mechanism of anti-inflammatory action. After treatment of RAW246.7 cells with 0–50  $\mu$ M compound **20** for 24 h (MTT test), the  $IC_{50}$  value was 22.62  $\mu$ M, which demonstrated that compound **20** showed strong inhibitory activity against cell proliferation of RAW264.7 cells. In order to further study the anti-inflammatory effect of compound **20**, the mRNA level (Fig. 2A) of iNOS, TNF- $\alpha$  and IL-6 in the LPS-stimulated RAW264.7 macrophages were detected with the addition of 0–40  $\mu$ M compound **20**. The real-time PCR results showed that, after LPS treatment, the transcription level of iNOS (Fig. 2B), TNF- $\alpha$  (Fig. 2C) and IL-6 (Fig. 2D) in RAW264.7 cells increased significantly ( $p < 0.01$ ). Excitingly, compound **20** significantly downregulated the LPS-stimulated transcription of iNOS, TNF- $\alpha$  and IL-6.

Next, we detected the effects of compound **20** on the expression of various inflammatory factors. LPS could stimulate RAW264.7 cells to

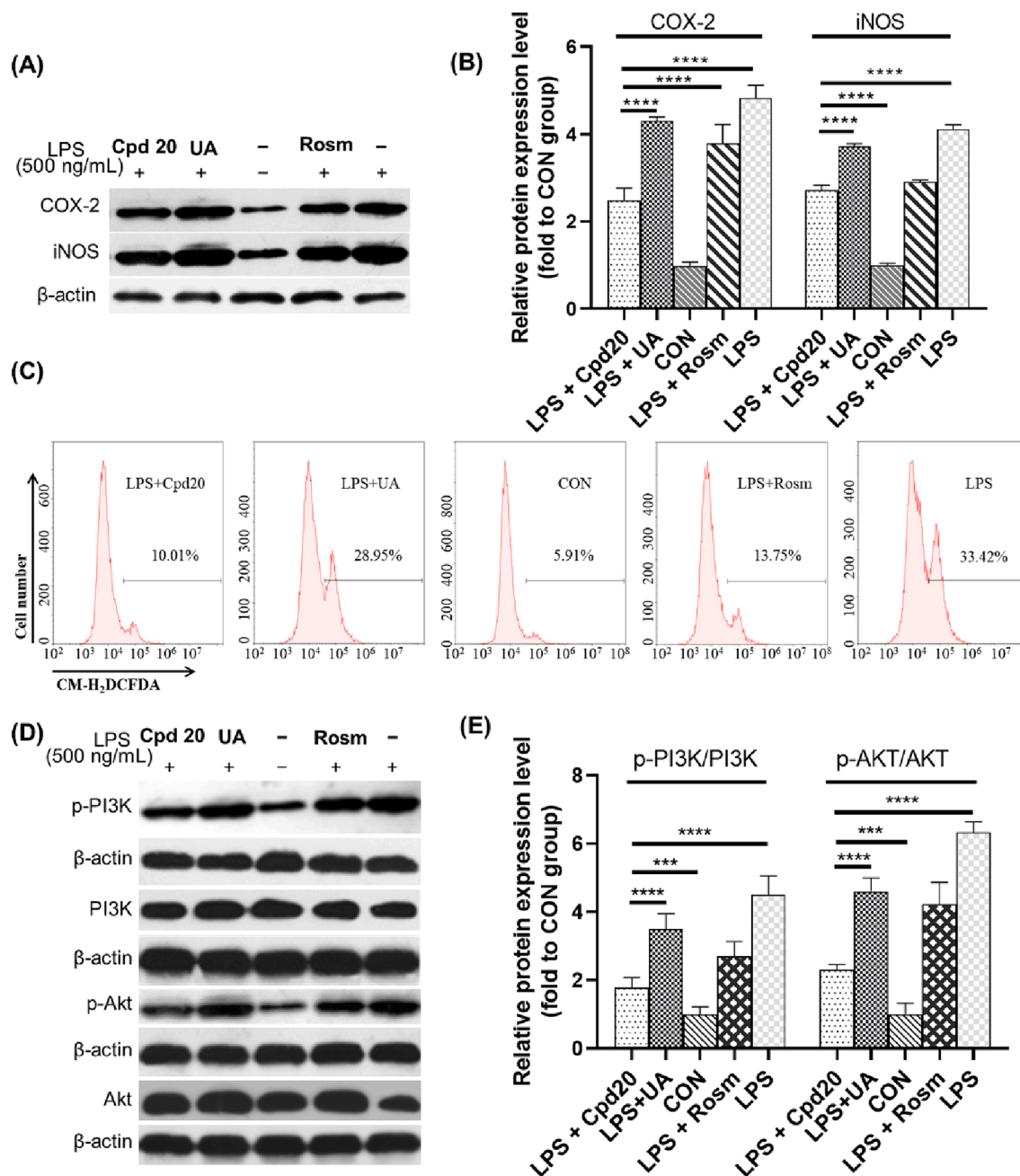


**Fig. 3.** Cpd20 reduces the LPS-induced ROS level through the PI3K/AKT signaling pathway. The relative expression level of COX-2, iNOS were detected by Western blot (A) and quantified (B); Intracellular ROS levels were measured by flow cytometry (C); and the relative expression level of PI<sub>3</sub>K/AKT signal pathway were detected by Western blot (D) and quantified (E). Values are expressed as mean ± SEM, n ≥ 3. \* Represents significant differences, \*\*\*p < 0.001, \*\*\*\*p < 0.0001.

produce large amounts of endogenous ROS, which mediated macrophage phagocytic functions and the transmission of inflammatory signals (Feng et al., 2018). Western blot detection results (Fig. 3A, B) showed that intracellular oxidation levels of iNOS and COX-2 were more significantly inhibited with compound 20 compared to UA treatment ( $p < 0.01$ ). Flow cytometry results revealed that compound 20 effectively down-regulated LPS-stimulated endogenous ROS accumulation in RAW264.7 cells (Fig. 3C) (LPS + Cpd 20 group vs LPS group,  $p < 0.01$ ). Previous studies have shown that activation of the PI3K/Akt/mTOR pathway is driven by ROS (Le Belle et al., 2011). Under the influence of LPS, phosphorylation level of PI3K and Akt were significantly increased (Fig. 3D, E). When RAW264.7 cells were co-treated with UA or compound 20, both PI3K and Akt phosphorylation levels were significantly inhibited. Compared to the LPS treatment, the  $p$ -PI<sub>3</sub>K/PI<sub>3</sub>K value

decreased by 40.3 % and 77.8 % with UA or compound 20, respectively, and the  $p$ -Akt/Akt value also decreased 36.5 % and 73 %, respectively (Fig. 3E). These results showed that compound 20 more effectively downregulated LPS-stimulated PI<sub>3</sub>K-Akt pathway activation. PI<sub>3</sub>K/AKT signalling pathway is important in cell proliferation, inflammatory response, and apoptosis (Owonikoko and Khuri, 2013, Mabuchi et al., 2015, Li et al., 2018). Akt is the downstream gene of PI<sub>3</sub>K, which can be activated by  $p$ -PI<sub>3</sub>K-induced phosphorylation ( $p$ -Akt).  $p$ -Akt can induce caspase-9 phosphorylation, blocking caspase-3 activation by caspase-9, and  $p$ -Akt can induce Bax expression, inhibit CHOP and JNK expression and activation, and inhibit endoplasmic reticulum stress pathway (Wu et al., 2018, Li et al., 2019). A large amount of endogenous ROS formed in RAW264.7 cells with the stimulation of LPS, mediated the phagocytic function of macrophages and the transmission of inflammatory signals

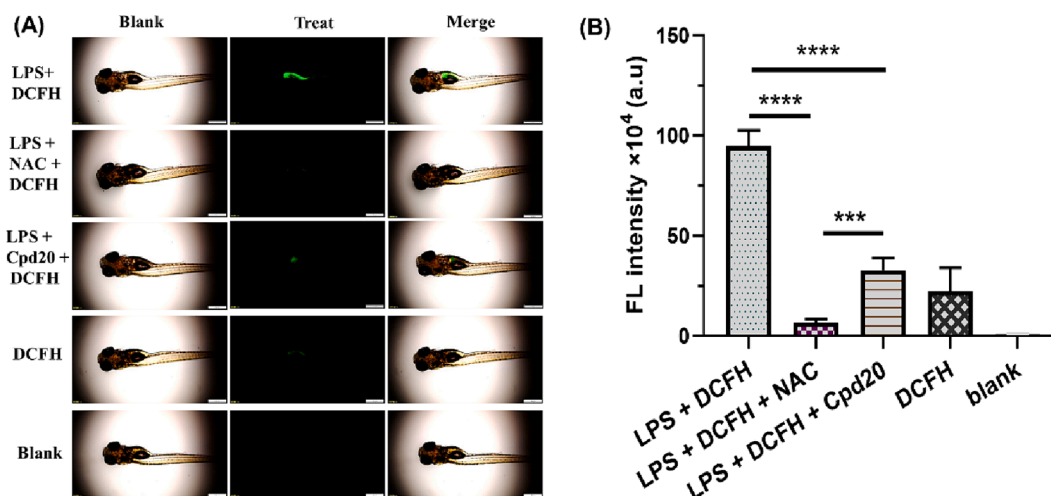


Fig. 4. Cpd20 treatment reduced the ROS level in LPS-induced zebrafish. The fluorescence image (A) and FITC intensity (B) of zebrafish  $\bullet$ OH was collected by FITC channel. The scale bar represents 500  $\mu$ m. Values are expressed as mean  $\pm$  SEM,  $n \geq 3$ . \* Represents significant differences, \*\*\* $p < 0.001$ , \*\*\*\* $p < 0.0001$ .

(Feng et al., 2018). In this study, the Western blot results of iNOS and COX-2 revealed that the ROS level was significantly inhibited after the addition of UA or compound 20. Furthermore, flow cytometry results revealed that the ROS level was significantly down-regulated after treatment with compound 20, which indicated that compound 20 principally presented a high anti-inflammation under the function of LPS-stimulated oxidative stress. Furthermore, Western blot-based assays revealed that leader compound 20 effectively inhibited the expression of inflammatory factors iNOS ( $p < 0.05$ ) and COX-2 ( $p < 0.01$ ), and blocked the LPS-activated PI<sub>3</sub>K/Akt signalling pathway *in vitro*, suggesting that triterpenoid-gallic hybrids may be potential contributions for PI<sub>3</sub>K/Akt signalling pathway in chronic inflammation. Accordingly, compound 20 possessed the biological activity of inhibiting LPS-stimulated oxidation and remarkably inhibited iNOS and COX-2 expression, and further inhibited PI3K-Akt signal pathway activation by down-regulating ROS levels.

### 3.5. Reduction of gastrointestinal tract hydroxyl radicals in LPS-stimulated zebrafish

To further testify the effectiveness of compound 20 anti-inflammation *in vivo*, an inflammation model from the gastrointestinal tract of LPS-stimulated zebrafish was implemented. We used the ratio-based fluorescent probe DCFH (2',7'-dichlorodihydrofluorescein diacetate) for gastrointestinal inflammation (mainly located in the gastrointestinal tract of zebrafish, and could image the  $\bullet$ OH generated by LPS stimulation) to perform the fluorescence (FL) imaging pre-experiment of zebrafish  $\bullet$ OH. Six-days old zebrafish larvae were cultured under the 4  $\mu$ g/mL LPS environment for 24 h to induce gastrointestinal inflammation and the production of ROS such as  $\bullet$ OH. Then probe (10  $\mu$ M) was added to the culture system for 4 h, and observed under fluorescence microscope. As shown in Fig. 4A–B, the fluorescence signal of the probe was mainly presented in the gastrointestinal tract of fish. The FL intensity of zebrafish imaging was weak ( $0.97 \pm 0.02$  %) without LPS stimulation, and the background fluorescence may come from the reaction with low concentrations of endogenous free radicals in the gastrointestinal tract (Yuan et al., 2019). When LPS was added into the culture system, the FL intensity of gastrointestinal tract was significantly enhanced to  $94.82 \pm 7.73$  %. With the treatment of LPS plus compound 20 (5  $\mu$ M), the fluorescence intensity was decreased to  $32.85 \pm 5.90$  % (Aviello and Knaus, 2017). Compared with LPS-treated alone, it was significantly decreased ( $p < 0.01$ ). Compound 20 significantly reduced inflammation in the gastrointestinal tract of zebrafish *in vivo*. It was revealed that compound 20 significantly reduced inflammation in the

gastrointestinal tract of zebrafish and had an excellent antioxidant/anti-inflammatory function. Eventually, compound 20 significantly decreased inflammation levels *in vivo* in the gastrointestinal tract of zebrafish. Fig. 4

## 4. Conclusion

In sum, 16 novel UA-GA derivatives modified at UA C-28 site were designed, and synthesized. The *in vitro* and *in vivo* anti-inflammatory activity of hybrids, as well as the *in vitro* cytotoxicity, were evaluated. The toxicity of UA can be eliminated by modifying the free carboxyl group in hybrids. The stability of new derivatives is ensured with the persistence to hydrolysis of the C-28 ester or amide bond between the triterpenoid and linker group as well as the ether linkage between the 1,2,3-triazole and gallate fragment. Moreover, due to the introduction of 1,2,3-triazole and gallate substituents, amphiphilic hybrids possessed excellent oxidation and inflammatory resistance. Leader compound 20 efficiently inhibited LPS-stimulated oxidation and remarkably decreased iNOS and COX-2 expression, and further inhibited PI3K-Akt signal pathway activation by down-regulating ROS levels. Therefore, the development of UA-GA hybrids may provide a chemical basis and anti-inflammatory mechanism for designing and optimizing more effective agents.

## CRediT authorship contribution statement

**Zhiwen Qi:** Conceptualization, Data curation, Formal analysis, Funding acquisition, Investigation, Methodology, Project administration, Resources, Software, Supervision, Validation, Visualization, Writing – original draft, Writing – review & editing. **Pujun Xie:** Funding acquisition, Methodology. **Zhihong Wang:** Data curation. **Hao Zhou:** Resources, Validation. **Ran Tao:** Formal analysis, Visualization. **Sergey A. Popov:** Data curation, Writing – review & editing. **Guliang Yang:** Methodology. **Elvira E. Shults:** Formal analysis, Writing – review & editing. **Chengzhang Wang:** Formal analysis, Writing – review & editing.

## Declaration of competing interest

The authors declare that they have no known competing financial interests or personal relationships that could have appeared to influence the work reported in this paper.

## Acknowledgments

We thank the National Key Research and Development Program of China (2022YFD2200604-3), National Natural Science Foundation of China (32101472; 32271820), Hunan Natural Science Foundation Project (2021JJ31154), and Russian Science Foundation (grant # 23-73-00077) for financial support. Authors would like to acknowledge the Multi-Access Chemical Research Center SB RAS for spectral and analytical measurements.

## References

- Al Zahrani, N.A., El-Shishtawy, R.M., Asiri, A.M., 2020. Recent developments of gallic acid derivatives and their hybrids in medicinal chemistry: a review. *European Journal of Medicinal Chemistry*. 204, 112609 <https://doi.org/10.1016/j.ejmech.2020.112609>.
- Al-kuraishy, H.M., Al-Gareeb, A.I., Negm, W.A., et al., 2022. Ursolic acid and SARS-CoV-2 infection: a new horizon and perspective. *Inflammopharmacology* 30, 1493–1501. <https://doi.org/10.1007/s10787-022-01038-3>.
- Aviello, G., Knaus, U.G., 2017. ROS in gastrointestinal inflammation: rescue or sabotage? *Br. J. Pharmacol.* 174, 1704–1718. <https://doi.org/10.1111/bph.13428>.
- Bilsborrow, J.B., Doherty, E., Tilstam, P.V., et al., 2019. Macrophage migration inhibitory factor (MIF) as a therapeutic target for rheumatoid arthritis and systemic lupus erythematosus. *Expert Opin. Ther. Targets* 23, 733–744. <https://doi.org/10.1080/14728222.2019.1656718>.
- Checker, R., Sandur, S.K., Sharma, D., et al., 2012. Potent anti-inflammatory activity of ursolic acid, a triterpenoid antioxidant, is mediated through suppression of NF- $\kappa$ B, AP-1 and NF-AT. *PLoS One* 7, e31318. <https://doi.org/10.1371/journal.pone.0031318>.
- Chen, X., Wan, Y., Zhou, T., et al., 2012. Ursolic acid attenuates lipopolysaccharide-induced acute lung injury in a mouse model. *Immunotherapy* 5, 39–47. <https://doi.org/10.2217/imt.12.144>.
- Csuk, R., Deigner, H.-P., 2019. The potential of click reactions for the synthesis of bioactive triterpenes. *Bioorg. Med. Chem. Lett.* 29, 949–958. <https://doi.org/10.1016/j.bmcl.2019.02.020>.
- Feng, G., Yang, X., Li, Y., et al., 2018. LPS enhances platelets aggregation via TLR4, which is related to mitochondria damage caused by intracellular ROS, but not extracellular ROS. *Cell. Immunol.* 328, 86–92. <https://doi.org/10.1016/j.cellimm.2018.04.002>.
- Gonzaga, D.T.G., Ferreira, L.B.G., Moreira Maramaldo Costa, T.E., et al., 2017. 1-aryl-1H- and 2-aryl-2H-1,2,3-triazole derivatives block P2X7 receptor in vitro and inflammatory response in vivo. *Eur. J. Med. Chem.* 139, 698–717. <https://doi.org/10.1016/j.ejmech.2017.08.034>.
- Habtemariam, S., 2019. Antioxidant and anti-inflammatory mechanisms of neuroprotection by ursolic acid: addressing brain injury, cerebral ischemia, cognition deficit, anxiety, and depression. *Oxid. Med. Cell. Longev.* 8512048. <https://doi.org/10.1155/2019/8512048>.
- Hawash, M., Jaradat, N., Hameedi, S., et al., 2020. Design, synthesis and biological evaluation of novel benzodioxole derivatives as COX inhibitors and cytotoxic agents. *BMC Chem.* 14, 54. <https://doi.org/10.1186/s13065-020-00706-1>.
- Jiang, W., Huang, R.-Z., Zhang, J., et al., 2018. Discovery of antitumor ursolic acid long-chain diamine derivatives as potent inhibitors of NF- $\kappa$ B. *Bioorg. Chem.* 79, 265–276. <https://doi.org/10.1016/j.bioorg.2018.05.005>.
- Ke, Y., Liang, J.-J., Hou, R.-J., et al., 2018. Synthesis and biological evaluation of novel Jiyuan Oridonin A-1,2,3-triazole-azole derivatives as antiproliferative agents. *Eur. J. Med. Chem.* 157, 1249–1263. <https://doi.org/10.1016/j.ejmech.2018.08.056>.
- Le Belle, J.E., Orozco, N.M., Paucar, A.A., et al., 2011. Proliferative neural stem cells have high endogenous ROS levels that regulate self-renewal and neurogenesis in a PI3K/Akt-dependent manner. *Cell Stem Cell* 8, 59–71. <https://doi.org/10.1016/j.stem.2010.11.028>.
- Li, H., Li, M., Xu, R., et al., 2019. Synthesis, structure activity relationship and in vitro anti-influenza virus activity of novel polyphenol-pentacyclic triterpene conjugates. *Eur. J. Med. Chem.* 163, 560–568. <https://doi.org/10.1016/j.ejmech.2018.12.006>.
- Li, Y., Xia, J., Jiang, N., et al., 2018. Corin protects H2O2-induced apoptosis through PI3K/AKT and NF- $\kappa$ B pathway in cardiomyocytes. *Biomed. Pharmacother.* 97, 594–599. <https://doi.org/10.1016/j.biopha.2017.10.090>.
- Li, H., Zhang, X., Qi, X., et al., 2019. Icaritin inhibits endoplasmic reticulum stress-induced neuronal apoptosis after spinal cord injury through modulating the PI3K/AKT signaling pathway. *Int. J. Biol. Sci.* 15, 277–286. <https://doi.org/10.7150/ijbs.30348>.
- Liang, J.-J., Yu, W.-L., Yang, L., et al., 2022. Design and synthesis of marine sesterterpene analogues as novel estrogen receptor  $\alpha$  degraders for breast cancer treatment. *Eur. J. Med. Chem.* 229, 114081 <https://doi.org/10.1016/j.ejmech.2021.114081>.
- Lipeeva, A.V., Dolgikh, M.P., Tolstikova, T.G., et al., 2020. A study of plant coumarins. 18. conjugates of coumarins with lupane triterpenoids and 1,2,3-triazoles: synthesis and anti-inflammatory activity. *Russ. J. Bioorg. Chem.* 46, 125–132. <https://doi.org/10.1134/S1068162020010161>.
- Liu, Y., Li, S., Gao, Z., et al., 2021. Indoleamine 2,3-dioxygenase 1 (IDO1) promotes Cardiac hypertrophy via a PI3K-AKT-mTOR-dependent mechanism. *Cardiovasc. Toxicol.* 21, 655–668. <https://doi.org/10.1007/s12012-021-09657-y>.
- Mabuchi, S., Kuroda, H., Takahashi, R., et al., 2015. The PI3K/AKT/mTOR pathway as a therapeutic target in ovarian cancer. *Gynecol. Oncol.* 137, 173–179. <https://doi.org/10.1016/j.ygyno.2015.02.003>.
- Owonikoko, T.K., Khuri, F.R., 2013. Targeting the PI3K/AKT/mTOR pathway: biomarkers of success and tribulation. *Am. Soc. Clin. Oncol. Educ. Book* e395–e401. [https://doi.org/10.14694/EdBook\\_AM.2013.33.e395](https://doi.org/10.14694/EdBook_AM.2013.33.e395).
- Popov, S.A., Wang, C., Qi, Z., et al., 2021a. Synthesis of water-soluble ester-linked ursolic acid-gallic acid hybrids with various hydrolytic stabilities. *Synth. Commun.* 1–12. <https://doi.org/10.1080/00397911.2021.1939057>.
- Popov, S.A., Wang, C., Qi, Z., et al., 2021b. Synthesis of water-soluble ester-linked ursolic acid-gallic acid hybrids with various hydrolytic stabilities. *Synth. Commun.* 51, 2466–2477. <https://doi.org/10.1080/00397911.2021.1939057>.
- Pucci, A., Albano, G., Pollastrini, M., et al., 2020. Supported tris-triazole ligands for batch and continuous-flow copper-catalyzed Huisgen 1,3-dipolar cycloaddition reactions. *Catalysts* 10, 434.
- Qi, Z., Yang, G., Deng, T., et al., 2021. Design and linkage optimization of ursane-thalidomide-based PROTACs and identification of their targeted-degradation properties to MDM2 protein. *Bioorg. Chem.*, 104901 <https://doi.org/10.1016/j.bioorg.2021.104901>.
- Quideau, S., Deffieux, D., Douat-Casassus, C., et al., 2011. Plant polyphenols: chemical properties, biological activities, and synthesis. *Angew. Chem. Int. Ed.* 50, 586–621. <https://doi.org/10.1002/anie.201000044>.
- Radtke, O.A., Kiderlen, A.F., Kayser, O., et al., 2004. Gene expression profiles of inducible nitric oxide synthase and cytokines in leishmania major-infected macrophage-like RAW 264.7 cells treated with gallic acid. *Planta Med.* 70, 924–928. <https://doi.org/10.1055/s-2004-832618>.
- Ryu, S.Y., Oak, M.-H., Yoon, S.-K., et al., 2000. Anti-allergic and anti-inflammatory triterpenes from the herb of *Prunella vulgaris*. *Planta Med.* 66, 358–360.
- Scotti, L., Ishiki, M.H., Ribeiro, F.F., et al., 2018. Computational studies applied to anti-inflammatory drug discovery: a review. *Curr. Org. Chem.* 22, 1673–1689. <https://doi.org/10.2174/1385272822666180906122934>.
- Shanmugam, M.K., Ong, T.H., Kumar, A.P., et al., 2012. Ursolic acid inhibits the initiation, progression of prostate cancer and prolongs the survival of TRAMP mice by modulating pro-inflammatory pathways. *PLoS One* 7, e32476.
- Silva, K.D.R.R., Sirasa, M.S.F., 2018. Antioxidant properties of selected fruit cultivars grown in Sri Lanka. *Food Chem.* 238, 203–208. <https://doi.org/10.1016/j.foodchem.2016.08.102>.
- Sultana, N., Saeed Saifi, Z., 2012. Naturally occurring and synthetic agents as potential anti-inflammatory and immunomodulators. *AntiInflammatory Antiallergy Agents Med Chem.* 11, 3–19. <https://doi.org/10.2174/187152312803476264>.
- Trivedi-Parmar, V., Jorgensen, W.L., 2018. Advances and insights for small molecule inhibition of macrophage migration inhibitory factor. *J. Med. Chem.* 61, 8104–8119. <https://doi.org/10.1021/acs.jmedchem.8b00589>.
- Wang, D., Etienne, L., Echeverria, M., et al., 2014. A highly active and magnetically recoverable Tris(triazolyl)-CuI catalyst for alkyne-azide cycloaddition reactions. *Chem – A European J.* 20, 4047–4054. <https://doi.org/10.1002/chem.201304536>.
- Wang, Y.-J., Lu, J., Wu, D.-M., et al., 2011. Ursolic acid attenuates lipopolysaccharide-induced cognitive deficits in mouse brain through suppressing p38/NF- $\kappa$ B mediated inflammatory pathways. *Neurobiol. Learn. Mem.* 96, 156–165. <https://doi.org/10.1016/j.nlm.2011.03.010>.
- Wu, X., Liang, Y., Jing, X., et al., 2018. Rifampicin prevents SH-SY5Y cells from rotenone-induced apoptosis via the PI3K/Akt/GSK-3 $\beta$ /CREB signaling pathway. *Neurochem. Res.* 43, 886–893. <https://doi.org/10.1007/s11064-018-2494-y>.
- Xie, Y.-D., Xu, Y.-H., Liu, J.-P., et al., 2021. 1,3-benzodioxole-based fibrate derivatives as potential hypolipidemic and hepatoprotective agents. *Bioorg. Med. Chem. Lett.* 43, 127898 <https://doi.org/10.1016/j.bmcl.2021.127898>.
- Yuan, G., Ding, H., Sun, H., et al., 2019. A mitochondrion-targeting turn-on fluorescent probe detection of endogenous hydroxyl radicals in living cells and zebrafish. *Sens. Actuators B* 296, 126706. <https://doi.org/10.1016/j.snb.2019.126706>.
- Zhang, T.-Y., Li, C.-S., Cao, L.-T., et al., 2021. New ursolic acid derivatives bearing 1,2,3-triazole moieties: design, synthesis and anti-inflammatory activity in vitro and in vivo. *Mol. Divers.* <https://doi.org/10.1007/s11030-021-10236-0>.
- Zhang, C., Xu, S.-H., Ma, B.-L., et al., 2017. New derivatives of ursolic acid through the biotransformation by *Bacillus megaterium* CGMCC 1.1741 as inhibitors on nitric oxide production. *Bioorg. Med. Chem. Lett.* 27, 2575–2578. <https://doi.org/10.1016/j.bmcl.2017.03.076>.
- Zhu, L., Gu, P., Shen, H., 2019. Gallic acid improved inflammation via NF- $\kappa$ B pathway in TNBS-induced ulcerative colitis. *Int. Immunopharmacol.* 67, 129–137. <https://doi.org/10.1016/j.intimp.2018.11.049>.